THE JOURNAL OF PHYSICAL CHEMISTRY A

Article

pubs.acs.org/JPCA

Deciphering the Structural Evolution and Electronic Properties of Magnesium Clusters: An Aromatic Homonuclear Metal Mg_{17} Cluster

Xinxin Xia,[†,‡] Xiaoyu Kuang,[*,†] Cheng Lu,[*,‡,§] Yuanyuan Jin,[†] Xiaodong Xing,[†] Gabriel Merino,[∥] and Andreas Hermann[*,⊥]

[†]Institute of Atomic and Molecular Physics, Sichuan University, Chengdu 610065, China

[‡]Department of Physics, Nanyang Normal University, Nanyang 473061, China

[§]Department of Physics and High Pressure Science and Engineering Center, University of Nevada, Las Vegas, Nevada 89154, United States

[∥]Departamento de Física Aplicada, Centro de Investigación y de Estudios Avanzados, Unidad Mérida, Km 6 Antigua Carretera a Progreso, Apdo. Postal 73, Cordemex, 97310 Mérida, Yucatán, Mexico

[⊥]Centre for Science at Extreme Conditions and SUPA, School of Physics and Astronomy, The University of Edinburgh, Edinburgh EH9 3JZ, United Kingdom

Supporting Information

ABSTRACT: The structures and electronic properties of low-energy neutral and anionic Mg_n (n = 3−20) clusters have been studied by utilizing a widely adopted CALYPSO structure searching method coupled with density functional theory calculations. A large number of low-energy isomers are optimized at the B3PW91 functional with the 6-311+G(d) basis set. The optimized geometries clearly indicate that a structural transition from hollow three-dimensional configurations to filled-cage-like structures occurs at n = 16 for both neutral and anionic clusters. Based on the anionic ground state structures, photoelectron spectra are simulated using time-dependent density functional theory (TD-DFT) and compared with experimental results. The good agreement validates that the current ground state structures, obtained from the symmetry-unconstrained searches, are true global minima. A detailed chemical bonding analysis distinctly indicates that the Mg_{17} cluster is the first neutral locally π-aromatic homonuclear all-metal cluster, which perfectly satisfies Hückel's well-known $4N + 2$ rule.

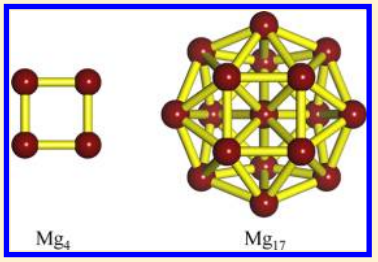

1. INTRODUCTION

Magnesium is an interesting metal that exhibits strong chemical activity. Its unique features have initiated extensive research in diverse fields such as superconductivity,[1] hydrogen storage,[2,3] nanomaterials,[4,5] and even biomedicine.[6] Apart from their direct influence in these fields, magnesium clusters exhibit a number of unique phenomena and features. One of the most striking phenomena is the transition from weak van der Waals bonding to metallic bonding as the clusters grow in size. The critical size for nonmetallic to metallic behavior was experimentally established to be n = 18 for anions,[7] and suggested to be n = 20 for neutral clusters.[8] From a theoretical perspective, the precise size of the insulator-to-metal transition is yet to be determined.[9−11]

There has been a plethora of theoretical studies on the geometric structures and electronic properties of magnesium clusters.[9−13] Jellinek et al.[9] investigated neutral and anionic magnesium clusters up to n = 22 using gradient-corrected density functional theory and found that the electron binding energies in the anionic clusters, derived from the gap between the two most external electrons, agree with electron photodetachment experiment data. Lyalin et al. investigated the structural evolution and electronic shells of neutral and cationic magnesium clusters using *ab initio* theoretical methods, where results showed that the metallic evolution is a slow and nonmonotonous process.[12] Exhaustive structure optimization revealed the growth behaviors of larger neutral magnesium clusters and indicated that most of the ground state structures are nonsymmetric in the size range n > 20.[13] It is worth pointing out that the neutral ground state structures found in the different studies are not identical.[9,12,13] Thus, although structures of magnesium clusters have been extensively studied and specific structures have been described and analyzed, the true ground state structures might still be debatable. Their electronic properties have been investigated by both experiment and theory, but these do not provide systematic information about their chemical bonding. It is therefore timely to (i) compare theoretical photoelectron spectra with the experimental PES to verify the lowest-energy structures of Mg clusters; (ii) investigate the most probable fragmentation channels for magnesium clusters; and (iii) understand the chemical bonding of Mg clusters, which also serve to explain their stabilizing mechanisms.

Received: July 21, 2016
Revised: September 7, 2016
Published: September 8, 2016

DOI: 10.1021/acs.jpca.6b07322
J. Phys. Chem. A 2016, 120, 7947−7954

To that end, we invoke the concept of aromaticity in our analyses. Aromaticity is traditionally confined to the realm of organic chemistry to describe cyclic, delocalized π bonding in planar and conjugate molecules possessing $(4N + 2)$ π electrons.[14−20] Recently, this concept has been extended to inorganic molecules including organometallic compounds,[21,22] transition-metal systems,[23−26] and in particular, all-metal clusters.[27−29] The gallium−gallium bond is exemplary for our understanding of electronic structure and chemical bonding in organometallic chemistry, with the first example of metalloaromaticity.[22] Combined anion photoelectron spectroscopy and quantum chemical calculations on metal−boron clusters indicated that various planar $M@B_n^-$ clusters feature planar aromatic boron rings, with delocalized π-electrons and the metal atom strongly covalently bound to the surrounding boron atoms.[23,24,30] A series of bimetallic metal anionic clusters with chemical composition MAl_4^- (M = Li, Na, or Cu) were synthesized and studied with photoelectron spectroscopy and *ab initio* calculations. This study showed that Al_4^{2-} maintains a square planar structure and aromaticity due to two delocalized π electrons present in all three MAl_4^- complexes.[27] Considering the concept of aromaticity, other small alkali metal and alkaline earth metal clusters were studied and for Li_2Mg_2 it was shown that the cyclic σ-aromatic structures are more stable than the classical linear Li−Mg−Mg−Li structure.[28] These investigation extended the aromaticity concept to the realm of all-metal species and highlighted its importance. Like aromaticity, which is then well-established in inorganic and all-metal systems, the concept of antiaromaticity (cyclic conjugated systems with $4N$ π electrons)[31] has recently been extended beyond organic molecules as well. The Al_4^{4-} anion in the $Li_3Al_4^-$ mixed-metal cluster was shown to feature π-antiaromaticity (and σ-aromaticity).[32,33] In recent years, three-dimensionalall-metal clusters, for instance, the Sb_4 unit in $[Ln(\eta^4\text{-}Sb_4)_3]^{3-}$ (Ln = La, Y, Ho, Er, Lu),[34] have been studied. On the basis of the results of chemical bonding analyses and Breslow's $4N$ rule, the $[Ln(\eta^4\text{-}Sb_4)_3]^{3-}$ (Ln = La, Y, Ho, Er, Lu) compound was found to be the first locally π-antiaromatic all-metal system. Despite aromaticity and antiaromaticity having been observed in inorganic and all-metal systems, these concepts have been applied relatively little to homonuclear metal clusters. However, it is mandatory to do an exhaustive and comparative study to establish if an all-metal aromatic cluster can be classified as aromatic.[35] With this in mind, the exploration of the geometric structures, electronic properties and the nature of the chemical bonding in magnesium clusters, is an intriguing proposition.

To study systematically and in-depth, the structural evolution and electronic properties of magnesium clusters, we have carried out comprehensive structure searches on neutral and anionic magnesium clusters in the size range from n = 3 to 20, by combining a systematic exploration of the potential energy surface using CALYPSO (Crystal structure AnaLYsis by Particle Swarm Optimization)[36−38] with density functional theory calculations. Subsequently, we reexamine the structure of particular neutral and anionic low-energy isomers of magnesium clusters with respect to those reported in previous experiments or theoretical calculations. We then study the stabilizing mechanism due to the electronic properties of specific neutral and anionic magnesium clusters and provide new insights for further theoretical and experimental explorations. The paper is organized as follows. The details of the computational method are presented in section II. Then, our results and discussion are described in section III. Finally, the main conclusions are summarized in secion IV.

2. COMPUTATIONAL DETAILS

The structures of low-lying isomers of neutral and anionic magnesium clusters were obtained using the CALYPSO method, which provides a local version of the particle swarm optimization (PSO) algorithm to explore the free-energy surfaces for any given (non)periodic system. The algorithm can predict stable structures depending only on the chemical composition. It has successfully predicted structures for various systems ranging from clusters[38] to surface reconstructions,[37,39] and crystal structures.[40,41] Here, structure predictions are performed for neutral and anionic magnesium clusters up to 20 atoms. Each generation contains 50 structures, 60% of which are generated by the PSO, whereas the others are new and will be generated randomly. We have followed 30 generations for each cluster to achieve convergence of the potential energy surface sampling. The searches generated 1000−1500 isomers for low-energy neutral and anionic magnesium clusters. Among those isomers, the 15 energetically lowest-lying isomers are selected as candidates for the global minimum structure. Low-energy structures within 3 eV of the global minimum structure are further optimized with subsequent frequency calculations. The calculations are performed using the all-electron density functional theory method with the B3PW91[42,43] generalized gradient approximation functional. The 6-311+G(d) basis set is selected for the confirmation of the lowest-energy structures of magnesium clusters. The choice of the B3PW91/6-311+G(d) level of theory set is based on a previous report.[12] The effect of spin multiplicity (up to septet and octet) is taken into account, and no symmetry constraints are enforced in the geometric optimization procedure. All calculations are performed with the Gaussian 09 program package.[44] The photoelectron spectra of the anionic magnesium clusters are simulated with the time-dependent density functional theory (TD-DFT) method. Chemical bonding analyses (B3PW91/6-311+G(d)) are conducted using the adaptive natural density partitioning (AdNDP)[45] method. The nucleus-independent chemical shift (NICS) and multicenter bond order are calculated by using the Multiwfn 3.3.8 program package.[46]

3. RESULTS AND DISCUSSION

3.1. Geometric Structure. We have performed a comprehensive structure search with the CALYPSO method and all of the previously reported structures, including experimental and theoretical ones, are successfully reproduced in our search results. On the basis of those results, we optimize the candidates of low-lying isomers and display the global minima structures of neutral and anionic magnesium clusters with up to 20 atoms in Figure 1. The vibrational frequencies are also calculated and listed in Table S1 (Supporting Information) to ensure true global minima for the ground state structures. Moreover, other typical low-energy isomers of all clusters, together with their corresponding symmetry, are displayed in Figure S1 (Supporting Information).

From Figure 1, we can see that the neutral and corresponding anionic magnesium clusters have similar ground-state structures and follow the same structural evolution. For both neutrals and anions, only the $Mg_3^{0/-}$ clusters are trigonal plane structures. For $n \geq 4$, the lowest-energy structures of magnesium clusters form three-dimen-

DOI: 10.1021/acs.jpca.6b07322
J. Phys. Chem. A 2016, 120, 7947−7954

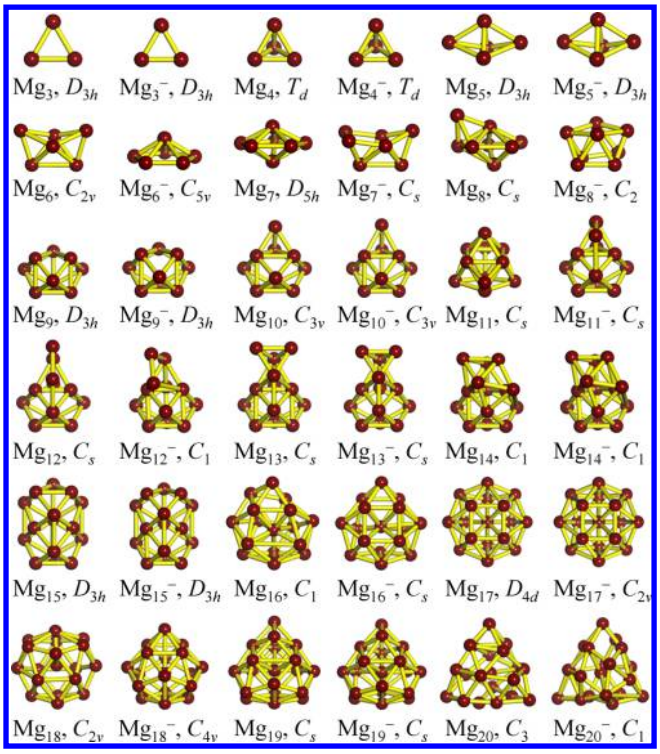

Figure 1. Lowest-energy structures of Mg_n^Q (n = 3−20; Q = 0, −1) clusters.

sional configurations. As the number of atoms increases, we find that eventually, for $n \geq 16$, one of the Mg atoms is fully encapsulated within the magnesium framework. So, n = 16 is a structural transition point from hollow three-dimensional configurations to filled-cage-like structures. All of the lowest-energy structures of neutral and anionic Mg_n^Q (n = 3−20, Q = 0, −1) clusters, except for $Mg_{14,16}$ and $Mg_{12,14,20}^-$, which are of C_1 symmetry, possess relatively high point symmetry. Additionally, it can be seen that for n = 3−5, 9, 10, 13, 15, 19 the neutral and anionic clusters have the same geometries and point symmetries.

The optimized lowest-energy structures found in our searches are largely in agreement with those discussed in earlier theoretical and experimental findings. However, we find an Mg_{13} cluster of C_s symmetry (Figure 1) to be the lowest-energy structure in our study, whereas the Mg_{13} cluster with C_1 symmetry (Figure S1), previously studied theoretically by Lyalin et al.,[12] is shown to be a transition state. For Mg_{19}, Lyalin et al.[12] claimed that global minimum structure has C_{2v} symmetry whereas our result found it to be of C_s symmetry, which is in agreement with the result reported by Heidari et al.[13] The structure of Mg_{20} is in agreement with the result of Jellinek et al.,[9] and different from that reported by Lyalin et al.[12] The global minimum structure of Mg_8^- is found here to be of C_2 symmetry, whereas the D_{4d} symmetry structure proposed by Jellinek et al.[9] is not the lowest-energy structure, as shown by the results of our harmonic vibration analysis. Note that the lowest-energy Mg_n^Q (n = 3−20, Q = 0, −1) clusters are found to prefer low spin state, except in the case of $Mg_{18}^{0/-}$ where the ground state are triplet and quartet, respectively. The spin states of all these lowest-energy clusters are in good agreement with the results of Acioli et al.[10]

3.2. Electronic Properties of Anionic Mg_n^- Clusters with Ground State Structures. To confirm the validity of the ground state structures (shown in Figure 1) of Mg_n^- (n = 3−20) clusters, their photoelectron spectra were simulated using TD-DFT. The simulated spectra of the ground state structures are displayed in Figure 2, along with the available experimental spectra[8] for comparison. Simulated spectra of other low-energy isomers are shown in Figure S2 in the Supporting Information. The vertical detachment energy (VDE) was taken from the first peak position of the spectra and the adiabatic detachment energy (ADE) for the neutral clusters was measured by the corresponding intersection between the baseline and the rising edge of the first peak. Comparing the calculated and experimental numbers in Table 1, we can see that both the VDE and the ADE values extracted from the simulated PES are in satisfactory agreement with the experimental data, supporting the reliability of our theoretical approach. The spectra themselves are in overall good agreement with experiment throughout, though spectral weight seems to be off in some cases ($Mg_{11,18,19}^-$). The photoelectron spectra for Mg_n^- with n = 3−13 show only one major peak in the range of low binding energy (≤2.0 eV), whereas several recognizable peaks are found in the binding energy range 2.0−3.3 eV. Notice that for cluster sizes n = 16−19 the VDE's are larger than 2.0 eV, followed by a drop to 1.88 eV for n = 20. From the simulated PES, evidently the energy spacing between the first two main spectral features, which can be interpreted as the HOMO−LUMO gap for neutral magnesium clusters, has a local maximum (compared to their neighbors' gaps) for n = 4, 10, and 20. This phenomenon is consistent with the neutral HOMO−LUMO gap analysis discussed below and offers a first hint toward stability of magic number clusters. Overall, the comparison of the experimental and simulated PES results lends support to the proposed ground state structures of magnesium clusters.

The experimental and theoretical values of ADE and VDE, listed in Table 1, have been plotted as a function of cluster size in Figure 3 to explore more deeply their electronic properties. The theoretical values of ADE increase from 0.80 to 1.89 eV for n = 3−9 (Figure 3a). Afterward, the theoretical ADE reveals obvious odd−even oscillation from n = 13 to 18. The theoretical ADEs successfully reproduce the overall experimental trend and yield two striking minima at n = 10 and 20, which are related to the shell model introduced by Thomas et al.[8] As shown in Figure 3b, the theoretical values of the VDE keep increasing overall with increased numbers of Mg atoms, and two obvious minima appear again at n = 10 and 20. Again, the calculated VDEs are in good agreement with the experimental results, with only n = 6, 12, 18, 19 deviating by more than 0.1 eV. Note that for most cluster sizes, the deviation between theoretical values of ADE and VDE is less than 0.13 eV, with exceptions n = 6−8, 11, and 18. This is in agreement with the observation that all clusters, except for $Mg_{6-8,11,18}$, basically retain the structural framework of the neutral ground state in the corresponding anionic cluster.

3.3. Relative Stabilities and HOMO−LUMO Gaps. The inherent stability of a given cluster might be determined by its binding energy (E_b) per atom that, for neutral and anionic magnesium clusters, can be defined as

$$E_b = \frac{(n-1)E(Mg) + E(Mg^Q) - E(Mg_n^Q)}{n} \qquad Q = 0, -1 \tag{1}$$

where E is the total energy of the corresponding atom or cluster. The calculated results of E_b are summarized in Table 1

DOI: 10.1021/acs.jpca.6b07322
J. Phys. Chem. A 2016, 120, 7947−7954

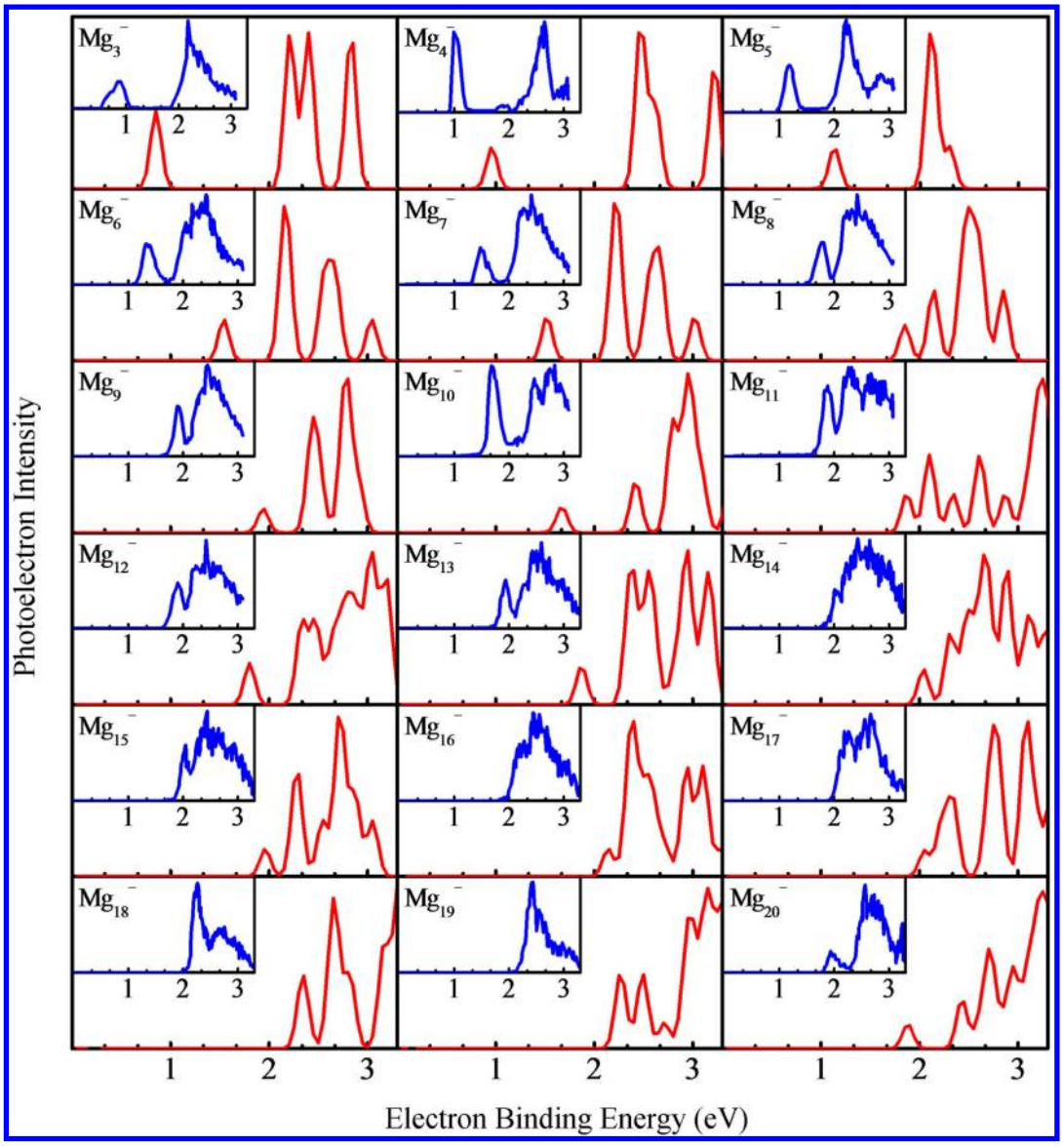

Figure 2. Comparison of the simulated photoelectron spectra (outer) with the experimental PES (inset) from ref 8 of lowest-energy Mg_n^- (n = 3−20) clusters.

and are plotted as a function of cluster size n in Figure 4a. For both the neutral and anionic magnesium clusters, the binding energies mostly increase with cluster size, and both curves show similar size dependence (Figure 4b). Three weak local peaks of the binding energy occur at n = 4, 10, and 15 for neutral clusters and n = 4, 9, and 15 for anionic clusters, respectively. This indicates that $Mg_{4,10,15}$ and $Mg_{4,9,15}^-$ are more stable than their adjacent sized clusters. It is also worth noticing that the E_b values of the anionic Mg_n^- cluster are always higher than their neutral counterparts. This implies that the binding energy of an additional electron is larger in the cluster than in a single Mg^- anion.

The second-order difference of the energy (Δ^2E) is another important parameter that can reflect the relative stabilities of neutral and anionic clusters and can be defined here as

$$\Delta^2E = E(Mg_{n-1}^{\ Q}) + E(Mg_{n+1}^{\ Q}) - 2E(Mg_n^{\ Q})$$
$$Q = 0, -1 \qquad (2)$$

The Δ^2E values for neutral and anionic Mg_n (n = 3−20) clusters are listed in Table S2 and shown in Figure 4b. Figure 4b reveals for both neutral and anionic clusters irregularly oscillating behavior in the region of n = 3−9 and odd−even oscillations for n = 12−18. Several pronounced peaks are found at n = 4, 7, 13, 15, and 17, signifying that the clusters $Mg_4^{\ 0/-}$, $Mg_7^{\ 0/-}$, $Mg_{13}^{\ 0/-}$, $Mg_{15}^{\ 0/-}$, and $Mg_{17}^{\ 0/-}$ are more stable compared to their neighbors. Furthermore, the neutral Mg_{10} and anionic Mg_9^- cluster are relatively more stable due to their locally maximal Δ^2E values.

The HOMO−LUMO gaps are calculated for the ground state $Mg_n^{\ Q}$ (n = 3−20, Q = 0, −1) structures. The energy gap between the highest occupied molecular orbital and the lowest unoccupied molecular orbital is an indicator of relative stability.[47] The results for the clusters in their ground state structures are summarized in Table 1 and plotted in Figure 4c. By comparing the E_{gap} values of neutral and anionic magnesium clusters, it can be seen that the E_{gap} curve for neutral clusters shows a decreasing trend with size, with significant fluctuations, whereas a much less pronounced trend is perceived for anionic

DOI: 10.1021/acs.jpca.6b07322
J. Phys. Chem. A 2016, 120, 7947−7954

Table 1. Calculated Binding Energies (E_b) and HOMO−LUMO Energy Gaps E_{gap} of the Lowest-Energy Mg_n^Q (n = 3−20; Q = 0, −1) Clusters and Data of Theoretical and Experimental Vertical Detachment Energies (VDEs) and Adiabatic Detachment Energies (ADEs) for the Lowest-Energy Mg_n^- (n = 3−20) Clusters (All Energies in eV)

	Mg_n		Mg_n^-		VDE		ADE	
n	E_b	E_{gap}	E_b	E_{gap}	theo	expt[a]	theo	expt[a]
3	0.13	2.86	0.45	1.09	0.85	0.83	0.80	0.60
4	0.30	2.89	0.58	1.18	0.96	0.96	0.96	0.96
5	0.30	2.16	0.55	1.20	1.13	1.19	1.07	1.04
6	0.31	1.98	0.54	1.16	1.54	1.38	1.23	1.23
7	0.37	2.09	0.58	1.16	1.52	1.50	1.32	1.35
8	0.40	1.78	0.62	1.11	1.85	1.81	1.61	1.60
9	0.48	1.53	0.71	1.15	1.94	1.91	1.89	1.80
10	0.54	1.96	0.71	1.31	1.67	1.68	1.54	1.55
11	0.53	2.04	0.68	1.17	1.87	1.88	1.50	1.60
12	0.53	1.43	0.68	1.02	1.80	1.91	1.71	1.70
13	0.55	1.45	0.70	1.02	1.87	1.94	1.79	1.80
14	0.55	1.21	0.71	0.97	2.04	2.01	1.99	1.92
15	0.60	1.22	0.74	0.90	1.96	2.03	1.90	1.90
16	0.60	1.03	0.74	1.00	2.14	2.16	2.09	2.10
17	0.66	1.10	0.78	0.83	2.05	2.11	1.99	2.00
18	0.68	1.06	0.81	1.13	2.37	2.23	2.12	2.15
19	0.70	0.99	0.82	1.00	2.28	2.43	2.18	2.21
20	0.72	1.52	0.82	0.94	1.88	1.93	1.75	1.78

[a]Reference 8.

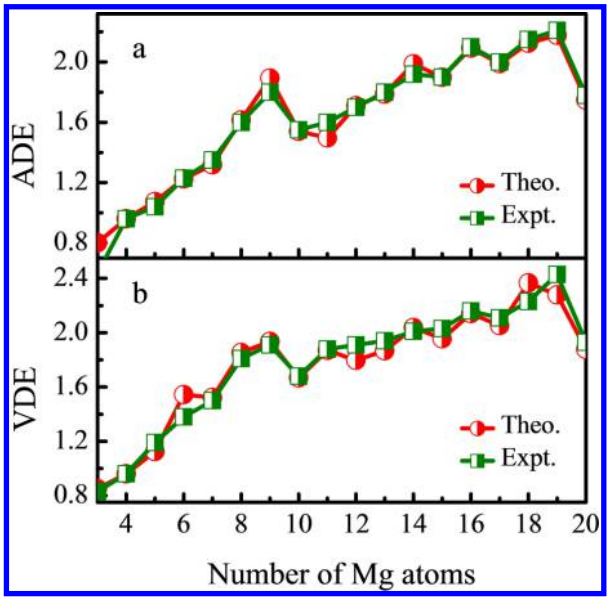

Figure 3. Adiabatic detachment energies (ADEs) and vertical detachment energies (VDEs) of Mg_n^- (n = 3−20) clusters: red circles, theory; green squares, experiment.

clusters. In addition, the values for neutral clusters are always higher than for anionic clusters, indicating that neutral Mg_n clusters are relatively more stable than anionic clusters. Local maxima values of E_{gap} are found at n = 4, 7, 11, 13, and 15 for neutral and n = 10, 16, and 18 for anionic clusters, respectively. This suggests that these cluster sizes have stronger stability than their size-adjacent clusters.

3.4. Fragmentation Channels. Potential fragmentation paths can be studied from a thermodynamic viewpoint (not

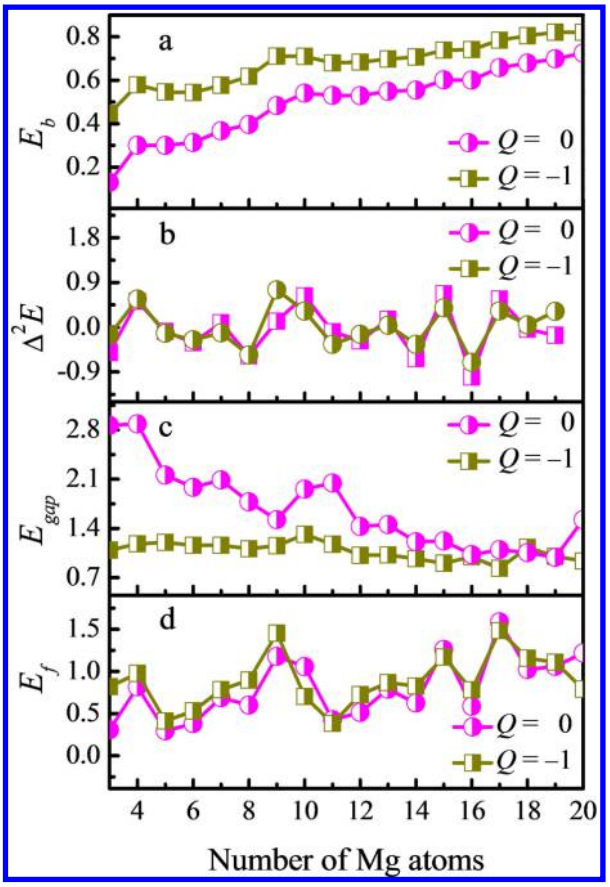

Figure 4. Averaged binding energies E_b (a), second-order energy differences Δ^2E (b), HOMO−LUMO energy gaps E_{gap} (c) and fragmentation energies of the most probable fragmentation channels (d) for lowest energy Mg_n^Q (n = 3−20, Q = 0, −1) clusters as functions of cluster size n.

considering kinetic barriers) and the fragmentation energies E_f of the ground state magnesium clusters can be expressed as

$$E_f = E(Mg_p) + E(Mg_{n-p}^Q) - E(Mg_n^Q) \qquad Q = 0, -1 \tag{3}$$

Generally speaking, if the fragmentation energy is negative for a particular fragmentation channel, the initial cluster is unstable and may dissociate spontaneously by releasing the amount of energy E_f. In this work, we have calculated all possible fragmentation channels for Mg_n^Q (n = 3−20, Q = 0, −1) clusters and the respective values are positive in all cases, implying that the clusters are stable and must obtain energy to realize the fragmentations. The smaller the fragmentation energies of cluster are, the less stable the clusters will be. The easiest (least energy-costly) fragmentation channels and corresponding fragmentation energies (E_f) for neutral and anionic magnesium clusters are summarized in Table 2. From the table, it is evident that the $Mg_n^Q \rightarrow Mg + Mg_{n-1}^Q$ channel is the most popular route for all neutral and anionic magnesium clusters. For clarity, the fragmentation energies of this most probable fragmentation channel are displayed in Figure 4d as functions of cluster size n. We notice that, except for n = 8, the two curves of fragmentation energies show quantitatively very similar behavior across the cluster sizes n = 3−18. Several energy maxima found at n = 4, 9, 15, and 17 suggest that initial clusters $Mg_4^{0/-}$, $Mg_9^{0/-}$, $Mg_{15}^{0/-}$, and $Mg_{17}^{0/-}$ are more stable than their neighbors and could be difficult to dissociate.

DOI: 10.1021/acs.jpca.6b07322
J. Phys. Chem. A 2016, 120, 7947−7954

Table 2. Easiest Fragmentation Channels and Corresponding Fragmentation Energies E_f for Mg_n^Q (n = 3−20; Q = 0, −1) Cluster

cluster	$Mg_p + Mg_{n-p}$	E_f (eV)	cluster	$Mg_p + Mg_{n-p}^-$	E_f (eV)
Mg_3	$Mg + Mg_2$	0.31	Mg_3^-	$Mg + Mg_2^-$	0.82
Mg_4	$Mg + Mg_3$	0.82	Mg_4^-	$Mg + Mg_3^-$	0.98
Mg_5	$Mg + Mg_4$	0.30	Mg_5^-	$Mg + Mg_4^-$	0.41
Mg_6	$Mg + Mg_5$	0.38	Mg_6^-	$Mg + Mg_5^-$	0.53
Mg_7	$Mg + Mg_6$	0.69	Mg_7^-	$Mg + Mg_6^-$	0.78
Mg_8	$Mg + Mg_7$	0.60	Mg_8^-	$Mg + Mg_7^-$	0.90
Mg_9	$Mg + Mg_8$	1.18	Mg_9^-	$Mg + Mg_8^-$	1.46
Mg_{10}	$Mg + Mg_9$	1.06	Mg_{10}^-	$Mg + Mg_9^-$	0.70
Mg_{11}	$Mg + Mg_{10}$	0.43	Mg_{11}^-	$Mg + Mg_{10}^-$	0.38
Mg_{12}	$Mg + Mg_{11}$	0.51	Mg_{12}^-	$Mg + Mg_{11}^-$	0.73
Mg_{13}	$Mg + Mg_{12}$	0.79	Mg_{13}^-	$Mg + Mg_{12}^-$	0.87
Mg_{14}	$Mg + Mg_{13}$	0.63	Mg_{14}^-	$Mg + Mg_{13}^-$	0.83
Mg_{15}	$Mg + Mg_{14}$	1.26	Mg_{15}^-	$Mg + Mg_{14}^-$	1.17
Mg_{16}	$Mg + Mg_{15}$	0.59	Mg_{16}^-	$Mg + Mg_{15}^-$	0.78
Mg_{17}	$Mg + Mg_{16}$	1.59	Mg_{17}^-	$Mg + Mg_{16}^-$	1.48
Mg_{18}	$Mg + Mg_{17}$	1.02	Mg_{18}^-	$Mg + Mg_{17}^-$	1.16
Mg_{19}	$Mg + Mg_{18}$	1.06	Mg_{19}^-	$Mg + Mg_{18}^-$	1.11
Mg_{20}	$Mg + Mg_{19}$	1.22	Mg_{20}^-	$Mg + Mg_{19}^-$	0.79

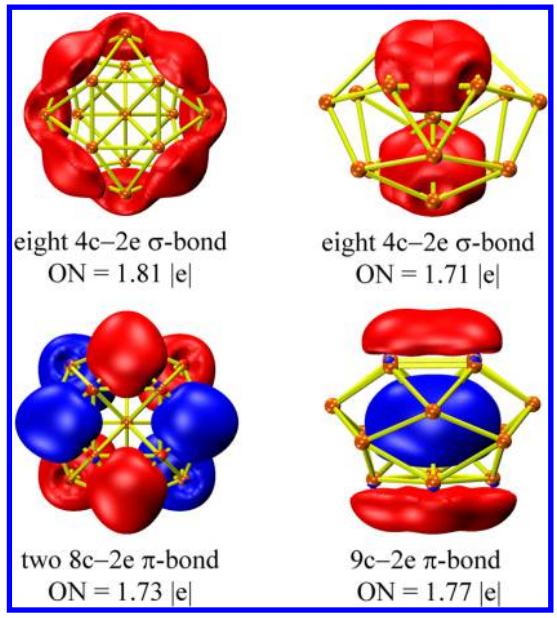

Figure 5. Chemical bonding analyses of neutral Mg_{17} cluster using the AdNDP method. ON stands for occupation number.

3.5. Chemical Bonding Analysis. From a comprehensive analysis of the electronic properties of the magnesium clusters, it is clear that the neutral Mg_{17} cluster is relatively stable, which caught our interest. The neutral cluster Mg_{17}, a filled-cage-like structure, has D_{4d} symmetry, four peripheral Mg_4 fragments, and one central Mg atom. To gain insight into its bonding properties, we analyzed the molecular orbitals (MO) of the neutral square Mg_4 unit (Figure S3a), which, as an isolated Mg_4 cluster, is a metastable species. The highest occupied MO (HOMO) of Mg_4 (Figure S3b) is a completely delocalized π orbital. There are also four lone-pair MOs and two pairs of σ electrons can be shared by four Mg−Mg bonds, resulting in an σ bond order of 0.5. Both the π bonding patterns and the lone-pair MOs of Mg_4 are analogous to the previously discovered aromatic Al_4^{2-} cluster.[27] In principle, the system satisfied the Hückel rule for a π-aromatic system. To provide further evidence for a possible aromatic character, we calculated its nucleus-independent chemical shift (NICS)[48,49] and multicenter bond order[50] (Table S3). NICS(0)_zz, NICS(0.5)_zz, and NICS(1)_zz are −37.1083, −36.5795, and −34.0287 ppm, respectively. All of the large negative NICS indices suggested that the Mg_4 cluster can be classified as aromatic. In addition, the total value of multicenter bond order is 0.0322, thus reconfirming the aromatic character of the Mg_4 cluster.

The ground state structure of neutral Mg_{17} found here contains two square Mg_4 frameworks. To improve our understanding of the bonding in the Mg_{17} cluster, we performed chemical bonding analyses using the AdNDP method. The detailed results are displayed in Figure 5. The 34 valence electrons in the neutral Mg_{17} cluster can be divided into two sets. The first set consists of delocalized σ-bond elements, whereas the other set is composed of delocalized π-bond elements. In the first set, the AdNDP analysis revealed eight 4c−2e σ-bonds with ON = 1.81 |e|, which are responsible for the bonding within the eight peripheral cyclo-Mg_4 units, and eight 4c−2e σ-bonds with ON = 1.71 |e|, which are likely due to the bonding between the central Mg with peripheral Mg_3 units. The second set includes two 8c−2e π-bonds, which are best described as two completely delocalized π bonds with 4 electrons in total and embody the strong bond among eight peripheral Mg atoms, and one 9c−2e π-bond with an occupation number (ON) of 1.77 |e|, which has an interesting sandwich shape and creates strains in the interior between the central Mg atom and the two apical Mg_4 units. The 9c−2e π-bonds on two Mg_4 units are quite similar to the 4c−2e bonds in the neutral square planar Mg_4 cluster (Figure S3c), which in turn are similar to the Sb_4 fragments of 5c−2e π-bonds in $[Ln(\eta^4\text{-}Sb_4)_3]^{3-}$ complex,[34] rendering it locally π-aromatic according to Hückel's $4N + 2$ rule. Why should such peculiar Mg_4 fragments occur in the Mg_{17} cluster? They are stabilized in Mg_{17} due to the strong interactions between the Mg_4 units and the central Mg atom and more importantly due to the presence of local aromaticity. Therefore, the neutral Mg_{17} cluster can be considered to be π-aromatic.

Moreover, the Mg_{17} cluster is a 34 electron system, which possesses a closed electronic shell according to the jellium superatom model.[51,52] For a detailed illustration of the electronic structure of the Mg_{17} cluster, we plotted its molecular orbitals (Figure S4). Combining the multicenter bonding and molecular orbitals analyses on the π-aromatic Mg_{17} cluster indicates that the electronic configuration of Mg_{17} can be labeled as $1S^21P^61D^42S^21D^61F^{14}$.

4. CONCLUSIONS

In summary, we have studied the structural evolution and electronic properties of neutral and anionic Mg clusters having up to 20 atoms using the unbiased CALYPSO structure searching method combined with density functional theory calculations. The ground state structures of both neutral and corresponding anionic Mg clusters have similar geometric structures and show the same structural evolution with increasing atom number. The simulated photoelectron spectra are in excellent agreement with experimental measurements. On the basis of fragmentation energy calculations, we identified that the $Mg_n^Q \rightarrow Mg_{n-1}^Q + Mg$ channel is the route favored by all the neutral and anion Mg_n clusters (n = 3−20) but is endothermic in all cases. A detailed chemical bonding analysis reveals that the neutral Mg_{17} cluster is the first locally π-

DOI: 10.1021/acs.jpca.6b07322
J. Phys. Chem. A 2016, 120, 7947−7954

aromatic cluster among medium-sized homonuclear metal clusters. To some extent, we expect that this result may provide a new twist on the concept of aromaticity and stimulate theoretical analyses of the chemical bonding in other known or as yet unknown homonuclear metal clusters.

■ ASSOCIATED CONTENT

Supporting Information

The Supporting Information is available free of charge on the ACS Publications website at DOI: 10.1021/acs.jpca.6b07322.

Low-lying isomers, vibrational frequencies, and second-order energy differences of neutral and anion Mg_n clusters, comparison of simulated and experimental PES, and chemical bonding analyses of the neutral Mg_4 cluster, molecular orbitals and energy levels of the neutral Mg_{17} cluster (PDF)

■ AUTHOR INFORMATION

Corresponding Authors

*X.Y.K. E-mail: scu_kuang@163.com. Telephone number: +86-28-85403803.

*C.L. E-mail: cheng.lu@unlv.edu. Telephone number: +1 702 957 2345.

*A.H. E-mail: a.hermann@ed.ac.uk. Telephone number: +44 131 650 5824.

Notes

The authors declare no competing financial interest.

■ ACKNOWLEDGMENTS

We thank Prof. Xiao Cheng Zeng at the University of Nebraska—Lincoln for useful discussion. This work was supported by the National Natural Science Foundation of China (No. 11274235, 11304167, 11574220, and 21671114), Program for Science & Technology InnovationTalents at the Universities of Henan Province (No.15HASTIT020), and Special Program for Applied Research on Super Computation of the NSFC-Guangdong Joint Fund (the second phase). The work in México was supported by Conacyt (Grant CB-2015-252356).

■ REFERENCES

(1) Monteverde, M.; Núñez-Regueiro, M.; Rogado, N.; Regan, K. A.; Hayward, M. A.; He, T.; Loureiro, S. M.; Cava, R. J. Pressure Dependence of the Superconducting Transition Temperature of Magnesium Diboride. *Science* **2001**, *292*, 75−77.

(2) Er, S.; Wijs, G. A. de; Brocks, G. Tuning the Hydrogen Storage in Magnesium Alloys. *J. Phys. Chem. Lett.* **2010**, *1*, 1982−1986.

(3) Nevshupa, R.; Ares, J. R.; Fernández, J. F.; del Campo, A.; Roman, E. Tribochemical Decomposition of Light Ionic Hydrides at Room Temperature. *J. Phys. Chem. Lett.* **2015**, *6*, 2780−2785.

(4) Chen, L. Y.; Xu, J. Q.; Choi, H.; Pozuelo, M.; Ma, X. L.; Bhowmick, S.; Yang, J. M.; Mathaudhu, S.; Li, X. C. Processing and Properties of Magnesium Containing a Dense Uniform Dispersion of Nanoparticles. *Nature* **2015**, *528*, 539−545.

(5) Barcaro, G.; Ferrando, R.; Fortunelli, A.; Rossi, G. Exotic Supported CoPt Nanostructures: From Clusters to Wires. *J. Phys. Chem. Lett.* **2010**, *1*, 111−115.

(6) Yoo, J.; Aksimentiev, A. Improved Parametrization of Li^+, Na^+, K^+, and Mg^{2+} Ions for All-Atom Molecular Dynamics Simulations of Nucleic Acid Systems. *J. Phys. Chem. Lett.* **2012**, *3*, 45−50.

(7) Diederich, T.; Döppner, T.; Braune, J.; Tiggesbäumker, J.; Meiwes-Broer, K. Electron Delocalization in Magnesium Clusters Grown in Supercold Helium Droplets. *Phys. Rev. Lett.* **2001**, *86*, 4807−4810.

(8) Thomas, O. C.; Zheng, W. J.; Xu, S. J.; Bowen, K. H., Jr. Onset of Metallic Behavior in Magnesium Clusters. *Phys. Rev. Lett.* **2002**, *89*, 213403.

(9) Jellinek, J.; Acioli, P. H. Magnesium Clusters: Structural and Electronic Properties and the Size-Induced Nonmetal-to-Metal Transition. *J. Phys. Chem. A* **2002**, *106*, 10919−10925.

(10) Acioli, P. H.; Jellinek, J. Electron Binding Energies of Anionic Magnesium Clusters and the Nonmetal-to-Metal Transition. *Phys. Rev. Lett.* **2002**, *89*, 213402.

(11) Köhn, A.; Weigend, F.; Ahlrichs, R. Theoretical Study on Clusters of Magnesium. *Phys. Chem. Chem. Phys.* **2001**, *3*, 711−719.

(12) Lyalin, A.; Solov'yov, I. A.; Solov'yov, A. V.; Greiner, W. Evolution of the Electronic and Ionic Structure of Mg Clusters with Increase in Cluster Size. *Phys. Rev. A: At., Mol., Opt. Phys.* **2003**, *67*, 063203.

(13) Heidari, I.; De, S.; Ghazi, S. M.; Goedecker, S.; Kanhere, D. G. Growth and Structural Properties of Mg_N (N = 10−56) Clusters: Density Functional Theory Study. *J. Phys. Chem. A* **2011**, *115*, 12307−12314.

(14) Hückel, E. Quantentheoretische Beiträge zum Benzolproblem. *Eur. Phys. J. A* **1931**, *70*, 204−286.

(15) Hückel, E. Quantentheoretische Beiträge zum Problem der aromatischen und ungesattigten Verbindungen. III. *Eur. Phys. J. A* **1932**, *76*, 628−648.

(16) Minkin, V. I.; Glukhovtsev, M. N.; Simkin, B. Y. *Aromaticity and Antiaromaticity*; John Wiley & Sons: New York, 1994.

(17) Zhang, A.; Han, Y. H.; Yamato, K.; Zeng, X. C.; Gong, B. Aromatic Oligoureas: Enforced Folding and Assisted Cyclization. *Org. Lett.* **2006**, *8*, 803−806.

(18) Jiang, J. Y.; Lima, O. V.; Pei, Y.; Zeng, X. C.; Tan, L.; Forsythe, E. Dipole-Induced, Thermally Stable Lamellar Structure by Polar Aromatic Silane. *J. Am. Chem. Soc.* **2009**, *131*, 900−901.

(19) Yang, Y. A.; Feng, W.; Hu, J. C.; Zou, S. L.; Gao, R. Z.; Yamato, K.; Kline, M.; Cai, Z. H.; Gao, Y.; Wang, Y. B.; Li, Y. B.; Yang, Y. L.; Yuan, L. H.; Zeng, X. C.; Gong, B. Strong Aggregation and Directional Assembly of Aromatic Oligoamide Macrocycles. *J. Am. Chem. Soc.* **2011**, *133*, 18590−18593.

(20) Boldyrev, A. I.; Wang, L. S. All-Metal Aromaticity and Antiaromaticity. *Chem. Rev.* **2005**, *105*, 3716−3757.

(21) Fernández, I.; Frenking, G.; Merino, G. Aromaticity of Metallabenzenes and Related Compounds. *Chem. Soc. Rev.* **2015**, *44*, 6452−6463.

(22) Robinson, G. H. Gallenes, Cyclogallenes, and Gallynes: Organometallic Chemistry about the Gallium-Gallium Bond. *Acc. Chem. Res.* **1999**, *32*, 773−782.

(23) Romanescu, C.; Galeev, T. R.; Li, W. L.; Boldyrev, A. I.; Wang, L. S. Transition-Metal-Centered Monocyclic Boron Wheel Clusters (M@Bn): A New Class of Aromatic Borometallic Compounds. *Acc. Chem. Res.* **2013**, *46*, 350−358.

(24) Li, W. L.; Jian, T.; Chen, X.; Chen, T. T.; Lopez, G. V.; Li, J.; Wang, L. S. The Planar $CoB1_{18}^-$ Cluster as a Motif for Metallo-Borophenes. *Angew. Chem.* **2016**, *128*, 1−6.

(25) Zubarev, D. Yu.; Averkiev, B. B.; Zhai, H. J.; Wang, L. S.; Boldyrev, A. I. Aromaticity and Antiaromaticity in Transition-Metal Systems. *Phys. Chem. Chem. Phys.* **2008**, *10*, 257−267.

(26) Galeev, T. R.; Boldyrev, A. I. Recent Advances in Aromaticity and Antiaromaticity in Transition-Metal Systems. *Annu. Rep. Prog. Chem., Sect. C: Phys. Chem.* **2011**, *107*, 124−147.

(27) Li, X.; Kuznetsov, A. E.; Zhang, H. F.; Boldyrev, A. I.; Wang, L. S. Observation of All-Metal Aromatic Molecules. *Science* **2001**, *291*, 859−861.

(28) Alexandrova, A. N.; Boldyrev, A. I. σ-Aromaticity and σ-Antiaromaticity in Alkali Metal and Alkaline Earth Metal Small Clusters. *J. Phys. Chem. A* **2003**, *107*, 554−560.

(29) Mercero, J. M.; Boldyrev, A. I.; Merinoc, G.; Ugalde, J. M. Recent Developments and Future Prospects of All-Metal Aromatic Compounds. *Chem. Soc. Rev.* **2015**, *44*, 6519−6534.

DOI: 10.1021/acs.jpca.6b07322
J. Phys. Chem. A 2016, 120, 7947−7954

(30) Islas, R.; Heine, T.; Ito, K.; Schleyer, P. v. R.; Merino, G. Boron Rings Enclosing Planar Hypercoordinate Group 14 Elements. *J. Am. Chem. Soc.* **2007**, *129*, 14767−14774.
(31) Breslow, R. Antiaromaticity. *Acc. Chem. Res.* **1973**, *6*, 393−398.
(32) Kuznetsov, A. E.; Birch, K. A.; Boldyrev, A. I.; Li, X.; Zhai, H. J.; Wang, L. S. All-Metal Antiaromatic Molecule: Rectangular Al_4^{4-} in the $Li_3Al_4^-$ Anion. *Science* **2003**, *300*, 622−625.
(33) Islas, R.; Heine, T.; Merino, G. Structure and Electron Delocalization in Al_4^{2-} and Al_4^{4-}. *J. Chem. Theory Comput.* **2007**, *3*, 775−781.
(34) Min, X.; Popov, I. A.; Pan, F. X.; Li, L. J.; Matito, E.; Sun, Z. M.; Wang, L. S.; Boldyrev, A. I. All-Metal Antiaromaticity in Sb_4-Type Lanthanocene Anions. *Angew. Chem., Int. Ed.* **2016**, *55*, 5531−5535.
(35) Hoffmann, R. The Many Guises of Aromaticity. *Am. Sci.* **2015**, *103*, 18.
(36) Wang, Y. C.; Lv, J.; Zhu, L.; Ma, Y. M. Crystal Structure Prediction via Particle-Swarm Optimization. *Phys. Rev. B: Condens. Matter Mater. Phys.* **2010**, *82*, 094116.
(37) Wang, Y. C.; Miao, M. S.; Lv, J.; Zhu, L.; Yin, K.; Liu, H. Y.; Ma, Y. M. An Effective Structure Prediction Method for Layered Materials Based on 2D Particle Swarm Optimization Algorithm. *J. Chem. Phys.* **2012**, *137*, 224108.
(38) Lv, J.; Wang, Y. C.; Zhu, L.; Ma, Y. M. Particle-Swarm Structure Prediction on Clusters. *J. Chem. Phys.* **2012**, *137*, 084104.
(39) Lu, S. H.; Wang, Y. C.; Liu, H. Y.; Miao, M. S.; Ma, Y. M. Self-Assembled Ultrathin Nanotubes on Diamond (100) Surface. *Nat. Commun.* **2014**, *5*, 3666.
(40) Wang, Y. C.; Ma, Y. M. Perspective: Crystal Structure Prediction at High Pressures. *J. Chem. Phys.* **2014**, *140*, 040901.
(41) Zhu, L.; Liu, H. Y.; Pickard, C. J.; Zou, G. T.; Ma, Y. M. Reactions of Xenon With Iron and Nickel are Predicted in the Earth's Inner Core. *Nat. Chem.* **2014**, *6*, 644−648.
(42) Becke, A. D. Density-Functional Thermochemistry. III. The Role of Exact Exchange. *J. Chem. Phys.* **1993**, *98*, 5648−5652.
(43) Perdew, J. P.; Wang, Y. Pair-distribution Function and its Coupling-Constant Average for the Spin-Polarized Electron Gas. *Phys. Rev. B: Condens. Matter Mater. Phys.* **1992**, *46*, 12947−12954.
(44) Frisch, M.; Trucks, G.; Schlegel, H.; Scuseria, G.; Robb, M.; Cheeseman, J.; Montgomery, J. A., Jr.; Vreven, T.; Kudin, K.; Burant, J.; et al. *Gaussian 09*, revision C.0; Gaussian, Inc.: Wallingford, CT, 2009.
(45) Zubarev, D. Y.; Boldyrev, A. I. Developing Paradigms of Chemical Bonding: Adaptive Natural Density Partitioning. *Phys. Chem. Chem. Phys.* **2008**, *10*, 5207−5217.
(46) Lu, T.; Chen, F. Multiwfn: A Multifunctional Wavefunction Analyzer. *J. Comput. Chem.* **2012**, *33*, 580−592.
(47) Pearson, R. G. The Principle of Maximum Hardness. *Acc. Chem. Res.* **1993**, *26*, 250−255.
(48) Schleyer, P. v. R.; Maerker, C.; Dransfeld, A.; Jiao, H. J.; Hommes, N. J. R. v. E. Nucleus-Independent Chemical Shifts: A Simple and Efficient Aromaticity Probe. *J. Am. Chem. Soc.* **1996**, *118*, 6317−6318.
(49) West, R.; Buffy, J. J.; Haaf, M.; Müller, T.; Gehrhus, B.; Lappert, M. F.; Apeloig, Y. Chemical Shift Tensors and NICS Calculations for Stable Silylenes. *J. Am. Chem. Soc.* **1998**, *120*, 1639−1640.
(50) Giambiagi, M.; de Giambiagi, M. S.; Mundim, K. C. Definition of a Multicenter Bond Index. *Struct. Chem.* **1990**, *1*, 423−427.
(51) De Heer, W. A. The Physics of Simple Metal Clusters: Experimental Aspects and Simple Models. *Rev. Mod. Phys.* **1993**, *65*, 611−676.
(52) Brack, M. The Physics of Simple Metal Clusters: Self-Consistent Jellium Model and Semiclassical Approaches. *Rev. Mod. Phys.* **1993**, *65*, 677−732.

DOI: 10.1021/acs.jpca.6b07322
J. Phys. Chem. A 2016, 120, 7947−7954